Theor Chem Acc (2011) 128:675–681
DOI 10.1007/s00214-010-0806-7

REGULAR ARTICLE

Origin of the size dependence of Au nanoparticles toward molecular oxygen dissociation

Alberto Roldán · Josep M. Ricart · Francesc Illas

Received: 21 July 2010 / Accepted: 23 August 2010 / Published online: 4 September 2010

Abstract Density functional theory calculations using a plane-wave basis set and a generalized gradient approach exchange-correlation potential have been carried out to study the dissociation of molecular oxygen by Au nanoparticles and its dependence with particle size. The analysis of the energy related data shows that the reactivity is dominated by the energy barrier height from adsorbed O_2 to the dissociated state and by the stability of molecular oxygen on the nanoparticle. The energy barrier is found to be only slightly dependent on the particles size where large variations are found for the adsorption energy of the O_2 molecule on the different nanoparticles. A careful analysis of the electronic structure shows that the driving force for O_2 adsorption by these nanoparticles is the existence of a clear gap between occupied and unoccupied states for the naked particle. This allows accommodating bonding states with O_2 below the Fermi level resulting in a strong interaction. On the contrary, the Au nanoparticles with a more metallic electronic structure have necessarily to accommodate bonding and antibonding states below the Fermi level with a concomitant weaker interaction with O_2.

Keywords Nanogold · Catalysis · O_2 dissociation

Published as part of the special issue celebrating theoretical and computational chemistry in Spain.

A. Roldán · F. Illas (✉)
Departament de Química Física & Institut de Química Teòrica i Computacional (IQTCUB), Universitat de Barcelona, C/Martí i Franquès 1, 08028 Barcelona, Spain
e-mail: francesc.illas@ub.edu

A. Roldán · J. M. Ricart
Departament de Química Física i Inorgànica, Universitat Rovira i Virgili, C/Marcel.lí Domingo s/n, 43007 Tarragona, Spain

1 Introduction

The physical properties and chemical reactivity of materials change in an interesting and often unexpected way as the sample size approaches nanoscale. One of the materials where such *nano* effect is most surprising is Au. It is nowadays well established that the otherwise noble metal becomes catalytically active when reaching the nanoscale regime to the point that this constitutes a new research field in catalysis [1–3] with important potential implications in chemical reactions of industrial interest [4]. New discoveries have been reported in the recent years for various reactions catalyzed by Au nanoparticles; in particular, we mention the technologically relevant water–gas shift reaction [5, 6], the difficult chemoselective hydrogenation of nitroaromatics under mild reaction conditions [7], and the selective oxidation of olefins [4, 8].

Undoubtedly, the most studied reaction catalyzed by Au nanoparticles is the low temperature CO oxidation by O_2, which takes place when the Au nanoparticles are supported on reducible metal oxides such as TiO_2, Fe_2O_3, CeO_2, and Co_3O_4 (see Ref. [9] and references therein). Here, one important step is molecular oxygen activation that occurs normally by partial electron transfer from the Au particle to the $2\pi^*$ antibonding molecular orbital of O_2 resulting in a noticeable elongation of the O–O bond. This follows the mechanism observed for several transition metal surfaces where molecular oxygen dissociation takes place directly or mediated by a chemisorbed O_2 species which acts as a precursor [10]. Even on the rather inactive MgO support, supported Au nanoclusters activate the adsorbed O_2 molecule to a peroxo-like species with a concomitant weakening of the O–O bond length that appears to be highly stretched when compared to the free molecule [11]. The activation is more pronounced when the Au nanoparticles

are supported on more active oxides such as TiO_2 but still without evidence of the presence of atomic oxygen [12–14]. Note, in passing by, that theoretical and experimental evidence for O_2 dissociation by very small Au nanoparticles has been recently reported although this implies using TiC as a support instead of an oxide [15]. Likewise, in a recent work, Schüth et al. [16] have shown that CO oxidation catalyzed by Au nanoparticles supported on MgO and $Mg(OH)_2$ can occur even below −70 °C although this requires supported Au clusters with sizes below 1 nm and the possible participation of atomic oxygen coming from the support. This is probably due to the difficulty to oxidize CO directly by O_2 at these low temperatures.

Part of the catalytic activity of Au nanoparticles arises from the concomitant increase in the ratio of surface to bulk atoms and from the appearance of new sites such as low coordinated atoms and those involving directly the support. The effect of low coordinated sites has been analyzed in detail and found to play a major role [14]. The relative abundance of low coordinated sites at its change with particle size [17], the metal–support interactions [11, 18], and the possible presence of quantum size effects [19] have all been considered by different authors but a clear cut analysis is still missing. A possible way to disentangle the different effects is to focus on the reactivity of Au nanoparticles of different size. The use of small enough Au nanoparticles containing a few atoms only allows one to investigate different low coordinated sites for molecular oxygen activation [20] but to avoid artifacts from the model it is convenient to search for all possible stable isomers and focus on the low-energy ones [21]. However, for larger nanoparticles, one can avoid the tedious structure search and already assume that the shape will be similar to the ones emerging from the simple Wulff construction [22]. This approach, first introduced to study Pd nanoparticles using a localized basis set and fully exploiting symmetry [23], has proven to be efficient in a plane-wave basis set implementation [24, 25] and followed in previous work analyzing the molecular mechanism of O_2 dissociation on Au clusters of increasing size [26]. One of the major findings of this work was the existence of a critical size for oxygen dissociation. This conclusion is based in the exploration of the potential energy surface showing that only for small particles such as Au_{25} or Au_{38} the energy barrier for O_2 dissociation is smaller than the O_2 desorption energy but without a clear cause for this fact. In order to find an explanation to this observation and motivated by the fact that the energy barrier for O_2 dissociation by Au nanoparticles is not largely affected by the particles size [26] and that charge effects rapidly vanish with the particle size [27], we have explored in detail the dependence of O_2 adsorption with respect to particle size and also considered explicitly a broader range particles. In particular, we consider particles with 13, 19, 38, 44, 55, 79, 85, 116, 140, 146, 147, 201, and 225 atoms. The detailed analysis of the electronic structure allowed us to identify the necessary condition for a given Au nanoparticle to activate molecular oxygen.

2 Models for Au nanoparticles and computational details

A systematic study of a large set of Au nanoparticles containing up to 225 atoms (Fig. 1) has been considered and their catalytic activity toward O_2 dissociation investigated using periodic density functional theory. The particles with $n = 13$, 19, 55, 79, 85, 116, 140, 146, 147, 201, and 225 have all a central atom surrounded by one or more complete shells while the particles with $n = 38$ and 44 have a central empty site surrounded by a first Au_6 octahedral shell. Note, however, that only in a few cases the outermost shell is complete leading to "full shell clusters" [28]. In these special cases, the total number of atoms for a particle with i complete shells (N_i) is given by Eq. 1

$$N_i = \sum_{i=1}^{n_{\text{shells}}} N_{i-1} + 10i^2 + 2 \tag{1}$$

with $N_0 = 1$ which leads to 13, 55, 147, 254 for $i = 1$, 2, 3, 4. This shell structure has to be kept in mind when analyzing the electronic structure of these nanoparticles because it results in a special stability, in agreement with the experimental evidence that these Au nanoparticles exhibit a particular chemical inertness [28]. All particles have nearly octahedral or cuboctahedral shape, and their atomic structure has been initially cut from the bulk so as to exhibit low-index planes. However, in a subsequent step (see below), their atomic structure has been fully optimized either in the absence or presence of a single oxygen molecule or two oxygen atoms arising from molecular oxygen dissociation. The full geometry optimization induces some

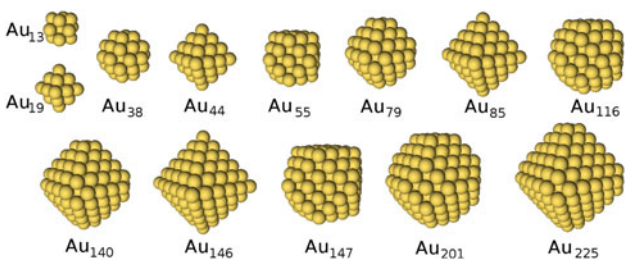

Fig. 1 Schematic representation of the structure of Au nanoparticles with octahedral or cuboactahedral shape containing 13, 19, 38, 44, 55, 79, 85, 116, 140, 146, 147, 201, and 225 atoms

deviation from the perfect octahedral or cuboctahedral initial form but the distortion is really small. The isolated single particles have been modeled by placing them in the center of a large enough supercell with a vacuum space of 1 nm in all directions to avoid interactions between replicated images in the neighboring cells. This supercell approach has been found to be an efficient way to study the atomic and electronic structure of rather large metallic nanoparticles [24, 25] with results of quality similar to those obtained from accurate all electron relativistic density functional calculations [23].

All calculations have been carried out using the VASP code [29], and the total energy has been computed using the generalized gradient approach (GGA) Perdew and Wang (PW91) potential [30]. Previous work using various GGA (PW91, PBE, and RevPBE) functionals has shown that qualitative trends are not affected by the choice of a particular form of the exchange-correlation potential [31] and, therefore, the choice of PW91 is appropriate. The effect of the core electrons on the valence electron density has been taken into account by the projector augmented wave (PAW) method of Blöch [32] as implemented in VASP [33]. The cutoff for the kinetic energy of the plane-wave basis set has been set to 415 eV. This is a typical value for the cutoff energy and ensures that the calculated energies are sufficiently converged. For these discrete systems, calculations have been carried out considering only the Γ-point of the reciprocal space. Geometry optimization was carried out using a gradient-conjugate method until forces on all atoms were less than 0.03 eV. A Gaussian smearing technique with a 0.05 eV width has been applied to enhance convergence but all energies presented below have been obtained by extrapolating to zero smearing (0 K). Finally, spin polarization has been taken into account to obtain the energy of the isolated O_2 molecule in its triplet ground state. The remaining calculations have been carried out without spin polarization since test calculations on various systems starting from spin polarized solutions always converted to the closed shell solution.

From the various possible ways of O_2 adsorption and dissociation on different sites of the particles, we have always considered the one which was found to be the minimum energy pathway in our previous work [26] and confirmed by the recent work of Boronat and Corma [34]. Transition state (TS) structures have been found using the climbing-image nudged elastic band (CI-NEB) [35] and DIMER [36] algorithms. All TS structures were fully characterized with a pertinent vibration analysis, neglecting coupling with the nanoparticle phonons, and making sure that the former have only positive eigenvalues and a single normal mode associated with an imaginary frequency.

3 Results and discussion

The chemical activity of extended metal surfaces is to a good measure given by the location of the d-band with respect the Fermi level [37, 38]. For discrete metal particles, it is more convenient to use the common concepts of frontier orbitals but the two points of view are intimately related as elegantly shown in the seminal book of Hofmann [39]. This is especially the case for rather large metallic particles where the proximity between the electronic levels results in a dense spectrum resembling that of the bulk material. In fact, for Au particles of $\sim$100 atoms, the density of states (DOS) plot obtained from a suitable smearing of the discrete levels appears to be close enough to the equivalent plot of bulk Au [25]. Therefore, DOS plots provide an easy and rather direct way to visualize the available states in the particle valence band near the Fermi level; this is the HOMOs, which can directly interact with the molecular oxygen orbitals. Table 1 collects the information of structure and DOS for the whole set of Au nanoparticles investigated in the present work and includes the equivalent data for the bulk. The analysis of data in Table 1 shows oscillations on the center of the d-band for the small particles and a monotonic, almost linear, trend to the bulk values for the 79 atom and larger particles, in agreement with previous work [25]. However, other properties such as Fermi level or density of states at the

Table 1 Geometrical details and electronic structure features of Au_n nanoparticles of increasing size (n = 13, 19, 38, 44, 55, 79, 85, 116, 140, 146, 147, 201, and 225)

n	Shape	N_{av}	Shells	d-band/eV	E_F/eV	DOS-E_F
13	Cub	4.62	1	−2.38	−4.88	2.85
19	Oct	6.32	1	−3.03	−4.33	0.39
38	Cub	7.58	2	−3.50	−3.51	0.68
44	Oct	7.64	2	−3.05	−4.61	0.71
55	Cub	7.85	2	−2.76	−4.70	0.41
79	Cub	8.51	3	−3.03	−3.84	0.62
85	Oct	8.47	3	−3.08	−4.29	0.67
116	Cub	8.90	3	−2.99	−3.95	1.37
140	Cub	9.09	3	−3.31	−3.51	0.30
146	Oct	9.04	3	−3.30	−3.97	0.39
147	Cub	8.98	3	−3.49	−2.51	0.50
201	Cub	9.43	4	−3.44	−3.06	0.33
225	Cub	9.49	4	−3.30	−3.97	0.44
Bulk	–	12.00	∞	−3.84	4.98	0.30

The table reports average coordination number (N_{av}), number of complete shells surrounding the central atom or empty site. The initial shape for octahedral and cuboctahedral particles is denoted as Oct and Cub, respectively. The center of the d-band respect to the Fermi level (E_F) is defined as d-band. Finally, DOS-E_F stands for the density of states at the Fermi level normalized with respect to the number of atoms. Equivalent information for bulk Au is included for comparison

Fermi level still present oscillations even for the largest particles.

The analysis presented for the electronic structure of the different Au nanoparticles above does not seem to offer a clue to understand the observed chemical differences toward molecular oxygen. However, from previous work, we know that Au_{38} is active toward O_2 dissociation and that, in addition, O_2 adsorption is large enough to allow dissociation before desorption. Clearly, this special behavior must be related to the electronic structure of this particle although this may not be evident. In order to confirm this hypothesis, we selected a subset of particles larger than Au_{38} but having atomic and electronic structure features as close as possible to those of Au_{38}. In particular we focus on particles with appropriate (100) facets because these are those exhibiting the active sites for O_2 dissociation as shown by different authors [26, 34] and with the location of the d-band center and the gap between the top of the d-band and the Fermi level close to the equivalent values for Au_{38}. From the long list of candidates on Table 1, Au_{116} and Au_{147} seem to exhibit the desired features; this will be later confirmed by the analysis of the density of states plots. We have then added Au_{55} and Au_{79} because they constitute clear examples of the opposite reactivity. For these particles the adsorption energy is smaller than the energy barrier for dissociation and consequently will not be able to dissociate O_2.

The properties relevant to O_2 activation in this series of nanoparticles are summarized in Table 2. These are the oxygen bond length elongation, arising mainly from the occupation of the O_2 ($2\pi^*$) molecular orbital, the net charge on the oxygen atoms, which is also related to the occupation of the O_2 ($2\pi^*$) orbital, the adsorption energy (E_{ads}), and the activation energy (E_a). The summary of results in Table 2 shows a direct relation between the charge transferred to the oxygen molecule and the elongation on the O–O bond. Note that the smallest amount of charge transfer corresponds to the Au_{55} particle which is simply due to its high ionization potential (see Table 1 and Ref. [27]). Interestingly enough, the activation energy does not strongly depend on the size of the nanoparticles, all values being in the 0.42–0.57 eV interval. However, the variation of the adsorption energy covers a much broader range, from −0.23 eV for Au_{55} to −0.96 eV for Au_{38}, as already found in previous work [26] but with interesting intermediate values such as −0.55 eV found for Au_{116}. The latter value is quite surprising since being at least of the order of the activation energy seems to contradict the previous conclusion that a critical size for the nanoparticles exists for O_2 dissociation. This conclusion was extracted from results for particles up to Au_{79} and from the fact that this particle size appears to be in the scalable regime, at least for the center of the d-band. The discussion above and the summary of results in Table 2 clearly indicate that the activation of the O_2 molecule by isolated (unsupported) Au particles is dominated by the magnitude of the adsorption energy of the O_2 molecule on a particular particle. In turn, the adsorption energy must depend on the mixing between frontier orbitals, that is, between the Au_n states near the Fermi level and the half occupied O_2 ($2\pi^*$) molecular

Table 2 Relevant quantities for the adsorption and dissociation of molecular oxygen on Au_n ($n = 38$, 55, 79, 116 and 147) nanoparticles

	d_{O-O}/Å	q_O/e	E_{ads}/eV	E_a/eV
Au_{38}	1.456	−0.43	−0.96	0.45
Au_{55}	1.364	−0.32	−0.23	0.54
Au_{79}	1.465	−0.44	−0.28	0.42
Au_{116}	1.440	−0.40	−0.55	0.51
Au_{147}	1.419	−0.40	−0.35	0.57

d_{O-O} and q_O stands for the O–O bond distance and the net charge on each oxygen atom in the molecularly adsorbed state and E_{ads} and E_a stand for the adsorption and activation energy toward O_2 dissociation, respectively

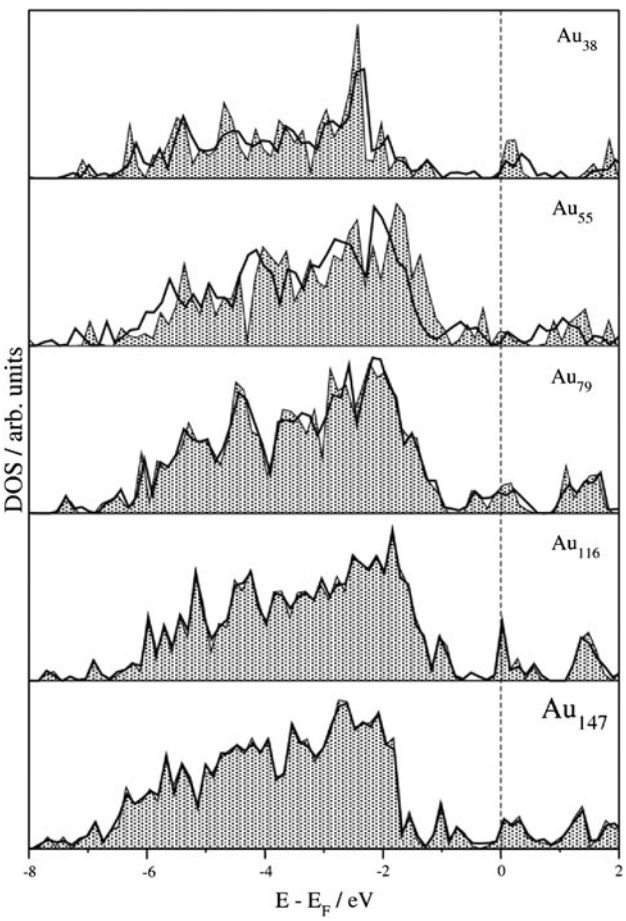

Fig. 2 Total density of states (*DOS*) of both Au_n (*dotted area*) and Au_n-O_2 systems (*thick solid line*) for the particle size corresponding to $n = 38$, 55, 79, 116, and 147

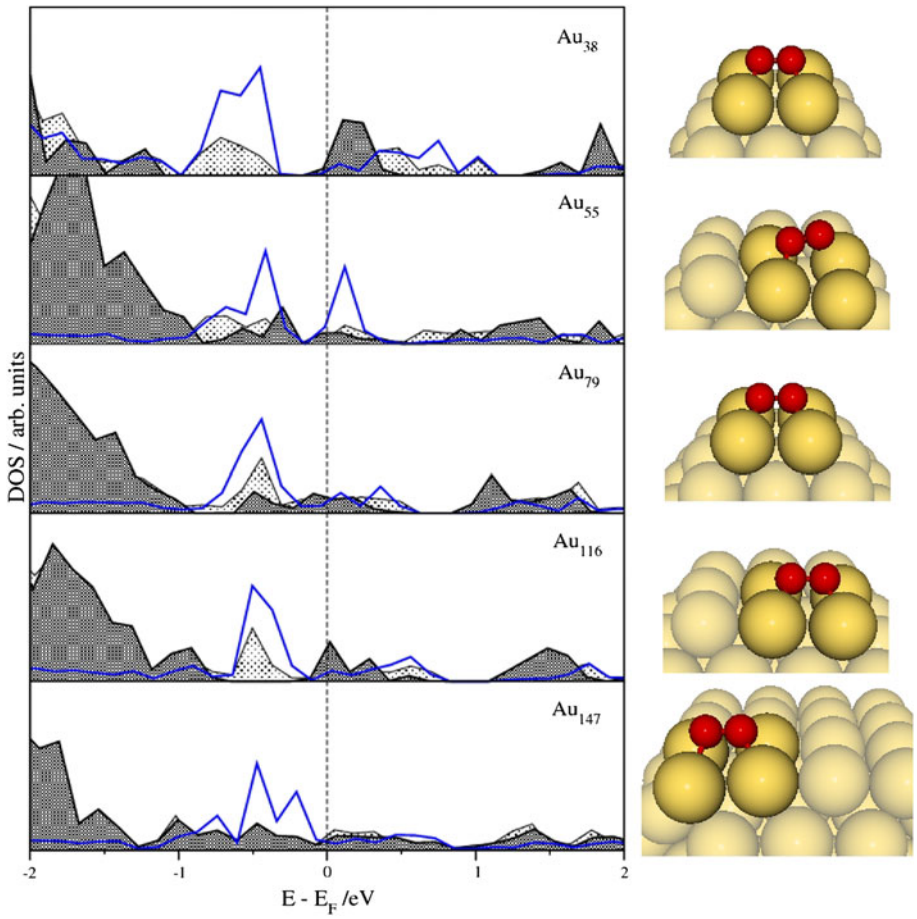

Fig. 3 Density of states (*DOS*) of Au_n-O_2 systems ($n = 38$, 55, 79, 116, 147) projected on the four interacting Au atoms (*dotted area*) and on the O_2 (*blue solid line*). The DOS plot of the same four atoms of bare nanoparticles (*dark area*) is given for comparison

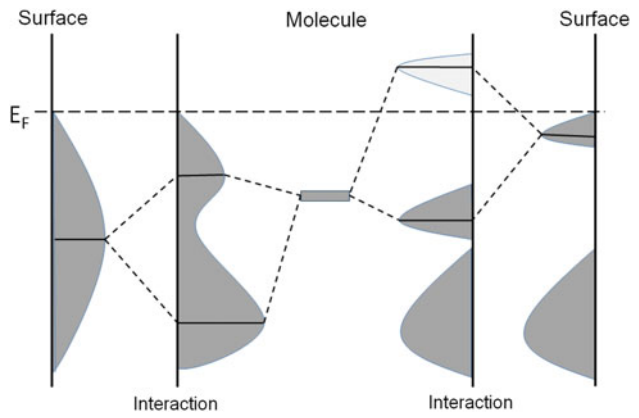

Fig. 4 Attractive molecule-metal interaction involving filled bonding states arising from mixing molecule and particle orbitals and empty antibonding states (*right*) and the opposite situation where bonding and antibonding states are both filled (*left*) resulting in a weak interaction

orbital. This hypothesis will be further analyzed in the forthcoming discussion.

A more detailed analysis of the arguments above can be obtained by inspection of the density of states (DOS) plots of the Au_n-O_2 systems compared to the Au_n bare ones. This allows one to have a broader perspective than the single value of the DOS at the Fermi level listed in Table 1. Figure 2 reports the corresponding DOS plots for $n = 38$, 55, 79, 116, and 147. Figure 2 also reports the DOS for the isolated Au_n particles and thus allows one to find whether the peaks of the DOS of the Au_n-O_2 systems coincide with those of the isolated particle as expected for a weak interaction with a concomitant low value of the adsorption energy or, on the contrary, are shifted thus indicating a stronger interaction. In the case of the Au_{38} particle, Fig. 2 shows that an Au-related peak near the Fermi level has been significantly shifted toward lower energies and evidences also a considerable mixing between the Au_{38} and O_2 states. This is in agreement with the large value of the calculated adsorption energy. Note, in addition, that the DOS of the bare Au_{38} particle has a noticeable density of states at the Fermi level which also contribute to the bonding states with molecular oxygen. For the larger Au_{55} and Au_{79} particles, the DOS at the Fermi level is significantly reduced and furthermore the projected DOS indicates that the mixing between Au_n and O_2 states is almost inexistent (see Fig. 3 and discussion below) Interestingly enough, the situation for Au_{116} closely resembles that of Au_{38} although with less marked features. Thus, in the

Au_{116} particle, there is a significant density of states near the Fermi level which also appears in the Au_{116}-O_2 system although significantly shifted toward lower energies.

A more detailed analysis of the DOS of the Au_n-O_2 systems is presented in Fig. 3 where the plot is made for the states near the Fermi level corresponding to the four Au atoms directly involved with the interaction with O_2. Figure 3 reveals that Au_{38} and Au_{116} states near Fermi level are significantly mixed with the O_2 states, mainly with the O_2 ($2\pi^*$) molecular orbitals resulting in bonding and antibonding states. Finally, both Au_{38} and Au_{116} have a marked molecular like electronic structure with a significant gap between the occupied states at levels below the Fermi level and those defining it. On the contrary, both Au_{55} and Au_{79} exhibit a more metallic electronic structure with a rather continuous and noticeably intense density of states up to the Fermi level. Consequently, Au_{38} and Au_{116} can accommodate bonding states below the Fermi level without filling the antibonding counterpart, whereas in the case of Au_{55} and Au_{79} bonding and antibonding states are occupied and, as a result, the interaction with O_2 is considerably reduced. This situation is illustrated schematically in the diagram in Fig. 4. For the cases where the DOS of bare Au_n shows a nearly continuous valence band, the interaction with occupied molecular orbital results in two states without gap between them. However, for the cases where there is a gap near Fermi level, the interaction results in filled bonding band and unoccupied antibonding band leading to stronger interaction.

4 Conclusions

Density functional theory calculations for the dissociation of molecular oxygen by Au nanoparticles of cuboacthedral shape and of increasing size shows that the reactivity is dominated by two main effects which are the energy barrier height from reactants to products and the stability of molecular oxygen on the nanoparticle. The energy barrier is found to be only slightly dependent on the particles size where large variations are found for the adsorption energy of the O_2 molecule on the different nanoparticles. A careful analysis of the electronic structure shows that the driving force for O_2 adsorption by these nanoparticles is the existence of a clear gap between occupied and unoccupied stated for the naked particle. This allows accommodating bonding states with O_2 below the Fermi level resulting in a strong interaction. On the contrary, the Au nanoparticles with a more metallic electronic structure have necessarily to accommodate bonding and antibonding states below the Fermi level with a concomitant weaker interaction with O_2. Hence particle size effects in the electronic structure caused by electron confinement to a restricted volume appear to be at the heart of the unexpected catalytic properties of the nanoscaled Au system in agreement with the recent results of Boyen et al. [40]. Finally, one must warn that the present conclusions have been extracted from a rather limited set of Au nanoparticles with cuboactahedral shape. Nevertheless, the frontier orbital analysis seems to indicate that the present conclusions are likely to be general and therefore to hold for nanoparticles with different shape although the precise reactivity will depend on the type of active site for O_2 dissociation.

Acknowledgments AR thanks *Universitat Rovira i Virgili*, for supporting his pre-doctoral research and FI acknowledges support received through the "2009 ICREA Academia" prize for excellence in research. Financial support has been provided by Spanish MICINN (grants FIS2008-02238 and CTQ2008-06549-C02-01) and in part by *Generalitat de Catalunya* (grants 2009SGR1041, 2009SGR00462 and XRQTC) and by COST Action D41 "Inorganic oxides: surfaces and interfaces". Computational time has been generously provided by the Barcelona Supercomputing Center.

References

1. Haruta M (1997) Catal Today 36:153–166
2. Valden M, Lai X, Goodman DW (1998) Science 281:1647–1650
3. See the articles in the special issue dedicated to chemistry of nanogold in Chem Soc Rev (2008) 37
4. Hughes MD, Xu YJ, Jenkins P, McMorn P, Landon P, Enache DI, Carley AF, Attard GA, Hutchings GJ, King F, Stitt EH, Johnston P, Griffin K, Kiely CJ (2005) Nature 437:1132–1135
5. Fu Q, Saltsburg H, Flytzani-Stephanopoulos M (2003) Science 301:935–938
6. Rodriguez JA, Ma S, Liu P, Hrbek J, Evans J, Perez M (2007) Science 318:1757–1760
7. Corma A, Serna P (2006) Science 313:332–334
8. Turner M, Golovko VB, Vaughan OPH, Abdulkin P, Berenguer-Murcia A, Tikhov MS, Johnson BFG, Lambert RM (2008) Nature 454:U931–U981
9. Herzing AA, Kiely CJ, Carley AF, Landon P, Hutchings GJ (2008) Science 321:1331–1335
10. Nolan PD, Wheeler MC, Davis JE, Mullins CB (1998) Acc Chem Res 31:798–804
11. Sanchez A, Abbet S, Heiz U, Schneider WD, Haekkinen H, Barnett RN, Landman U (1999) J Phys Chem A 103:9573–9578
12. Molina LM, Hammer B (2005) Appl Catal A 291:21–31 and references therein
13. Lopez N, Janssens TVW, Clausen BS, Xu Y, Mavrikakis M, Bligaard T, Norskov JK (2004) J Catal 223:232–235
14. Remediakis IN, Lopez N, Norskov JK (2005) Appl Catal. A 291:13–20
15. Rodríguez JA, Feria L, Jirsak T, Takahashi Y, Nakamura K, Illas F J Am Chem Soc 132:3177–3186
16. Jia C-J, Liu Y, Bongard H, Schüth F (2010) J Am Chem Soc 132:1520–1522
17. Mavrikakis M, Stoltze P, Norskov JK (2000) Catal Lett 64:101–106
18. Sterrer M, Yulikov M, Fischbach E, Heyde M, Rust HP, Pacchioni G, Risse T, Freund HJ (2006) Angew Chem Int Ed 45:2630–2632
19. Mills G, Gordon MS, Metiu H (2003) J Chem Phys 118:4198–4205

20. Tielens F, Andres J, Van Brussel M, Buess-Hermann C, Geerlings P (2005) J Phys Chem B 109:7624–7630
21. Davran-Candan T, Gunay ME, Yildirim R J Chem Phys 132: 174113-174129
22. Wulff G (1901) Z Krystallograph Mineral 34:449–530
23. Yudanov IV, Sahnoun R, Neyman KM, Rosch N (2002) J Chem Phys 117:9887–9896
24. Vines F, Illas F, Neyman KM (2008) J Phys Chem A 112:8911–8915
25. Roldan A, Vines F, Illas F, Ricart JM, Neyman KM (2008) Theor Chem Acc 120:565–573
26. Roldan A, Gonzalez S, Ricart JM, Illas F (2009) Chem Phys Chem 10:348–351
27. Roldán A, Ricart JM, Illas F, Pacchioni G (2010) Phys Chem Chem Phys. doi:10.1039/C004110F
28. Schmid G (2008) Chem Soc Rev 37:1909–1930
29. Kresse G, Furthmuller J (1996) Comput Mater Sci 6:15–50
30. Perdew JP, Burke K, Ernzerhof M (1996) Phys Rev Lett 77:3865–3868
31. Roldan A, Ricart JM, Illas F (2009) Theor Chem Acc 123:119–126
32. Blochl PE (1994) Phys Rev B 50:17953–17979
33. Kresse G, Joubert D (1999) Phys Rev B Condens Matter Mater Phys 59:1758–1775
34. Boronat M, Corma A (2010) Dalton Trans. doi:10.1039/c002280b
35. Henkelman G, Uberuaga BP, Jonsson H (2000) J Chem Phys 113:9901–9904
36. Henkelman G, Jonsson H (1999) J Chem Phys 111:7010–7022
37. Hammer B, Norskov JK (1995) Nature 376:238–240
38. Jiang T, Mowbray DJ, Dobrin S, Falsig H, Hvolbaek B, Bligaard T, Norskov JK (2009) J Phys Chem C 113:10548–10553
39. Hoffmann R (1989) Solids and surfaces. Wiley, New York
40. Boyen HG, Kastle G, Weigl F, Koslowski B, Dietrich C, Ziemann P, Spatz JP, Riethmuller S, Hartmann C, Moller M, Schmid G, Garnier MG, Oelhafen P (2002) Science 297:1533–1536